Applied Chemical Engineering (2021) Volume 4 Issue 1
doi:10.24294/ace.v4i1.802

ORIGINAL RESEARCH ARTICLE

The role of dysprosium ions as a dopant on linear and nonlinear optical dispersion parameters in a-Se thin film

Fathy A. Abdel-Wahab*, Heba Abdel Maksoud

Physics department, Faculty of Science, Ain Shams University, Abbassia, Cairo, Egypt. E-mail: fabdelwahab2003@yahoo.com

ABSTRACT

Thin films of un-doped and doped a-Se with Dysprosium rare-earth ions have been prepared by the thermal evaporation technique. The optical transmission spectra of the investigated films have been measured in a wide spectral range and used to calculate the linear optical constants together with the optical energy gap of studied films. The observed decrease in the values of the energy gap against the increase of the Dysprosium (Dy) content in a-Se films has been explained using Mott and Davis Model and in terms of electronegativity difference of the constituent atoms. Furthermore, the dispersion of nonlinear parameters such as second-order refractive index and nonlinear absorption coefficient (two-photon absorption coefficient) of investigated films are presented and discussed.

***Keywords*:** Selenium Thin Films; Doping of Selenium; Rare Earth; Optical Properties of Doped Selenium

ARTICLE INFO

Received: 7 April 2021
Accepted: 1 June 2021
Available online: 5 June 2021

1. Introduction

Rare-earth (RE)-doped glass fiber amplifiers operating at a 1.3 μm wavelength band have received extensive attention due to the zero-dispersion of the silica fiberglass in the 1.3 μm-wavelength region, and most installed fibers worldwide are optimized at this wavelength[1-4]. In contrast, Dysprosium rare-earth atoms, Dy which have an active unfilled f shell in its electronic configuration ([Xe] $4f^{10}4s^2$), can provide 1.3 μm emission due to the $^6F_{11/2}$, $^6H_{9/2}\rightarrow{}^6H_{15/2}$ transition[5]. In addition, Dy has a good absorption band at approximately 800 nm, at which level a cheap commercial laser diode could be used for excitation. On the other hand, amorphous Selenium (a-Se) is characterized by the existence of localized states in its mobility gap. These states are created due to the presence of structural defects and the absence of long-range order[6–8]. The structural disorder made a-Se and its alloys have high optical transparency in the infra-red (IR) spectral regions up to 10 μm. Besides, it has a large refractive index, thermal stability, and a high degree of covalent bonding. Furthermore, due to high rare-earth solubility, high emission quantum efficiency[9], and the low phonon energy (~ 250 cm^{-1}) of amorphous selenides compared with fluorides (~ 550 cm^{-1}), or oxide glasses (~ 1100 cm^{-1})[10], it could be used as a suitable host medium for Dy ions to enhance its mid-IR laser emission. It should be noted that the low phonon energy of a-Se decreases the multi phonon relaxation which enables an active transition between rare-earth atom levels in the middle IR spectral region. Consequently, the exploration of the optical properties of doped a-Se with Dy ions is very important to improve the performance of Laser emission[11].

In the previous work[12], the study of Selenium films was intended to have a comprehensive understanding of the influence of Dysprosium (Dy) ion dopant on the ac conductivity and dielectric parameters of a-Se films. The present aims to gain a better investigation on the effect of doping with Dy on the optical dispersion relations of the complex dielectric constant, optical energy gap, and material dispersion. Furthermore, the effect of doping of a-Se with Dy ions on second-order refractive index and two-photon absorption is calculated and discussed.

2. Experimental details

Bulk selenium doped with Dysprosium with ratios 0.008 and 0.01 at. % were prepared by mixing suitable proportions of Se and Dy, of purity 5 N, in a silica tube sealed at 10-5 Torr. The mixture was heated in an electric furnace up to 950 °C and kept at that temperature for 9 h. The obtained bulk ingots are used as source material to prepare thin films by the thermal evaporation technique. More details about bulk and thin films preparation of Se doped Dy are given elsewhere[12]. After evaporation, the thickness of the fresh films was accurately determined by an optical interference method and is found to be in the range of 750-804 nm.

The structural phase of as-prepared thin film samples has been identified using an X-ray diffraction pattern (XRD) computerized system (model: Philips EXPERT-MPDUG PW-3040 diffractometer with Cu Ka radiation source). The computer-aided two-beam spectrophotometer of type Shimadzu-3101PC UV-VIS-NIR, is used to record the optical transmittance (T) as a function of wavelength (λ) for the investigated films. A resolution limit of 0.2 nm and a sampling interval of 2 nm was utilized for recording the different measuring points. The accuracy of measuring $T(\lambda)$ is 0.003 with the incident beam at normal incidence to the film surface. The optical measurements were carried out at room temperature in the spectral region of 500-2500 nm.

3. Results and discussion

The recorded XRD patterns for the studied as-prepared a-Se, previous work of $SeDy_{0.008}$ films[12], and the present work [p. w.] of Se films doped with 0.01 at. % with Dy is shown in **Figure 1**. In this figure, the XRD pattern of the fresh Se films reflects its amorphous nature. The observed diffraction peaks in case of Se doped with 0.008 at. % Dy[12] means the growth of the crystalline phase at the expense of an amorphous state. This crystalline phase consists of mixed phases of elemental Se, Dy, and tetragonal and orthorhombic structures of SeDy as shown in **Figure 1**. Furthermore, increasing the Dy content in a-Se up to 0.01 at. % increased the intensity of the diffraction peaks for (102) of Dy and (002), (003), and (112) phases for SeDy which means that increasing the growth of crystalline zones in $SeDy_{0.01}$ as shown in **Figure 1**.

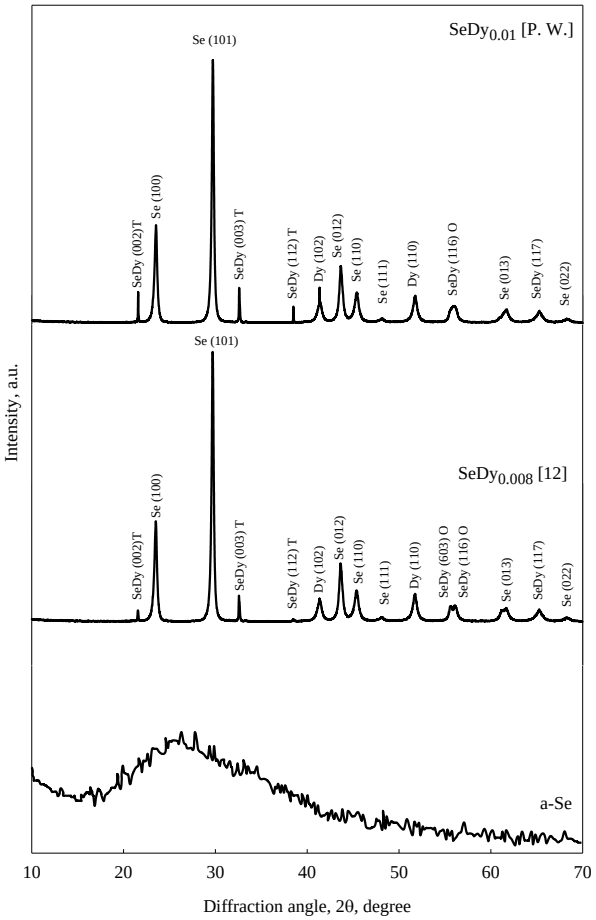

Figure 1. XRD pattern for a-Se, previous work of $SeDy_{0.008}$[12] and the present work [P.W.] of $SeDy_{0.01}$ thin films. It should be noted that the diffraction pattern of $SeDy_{0.008}$[12] is added to the figure for the sake of comparison.

3.1 Linear optical dispersion

The linear (weak field) optical constants such as refractive index (n), extinction coefficient (k), and optical energy gap, E_g, are considered as key parameter for optimizing the optical properties of a given optical application[13]. The measured optical transmission against wavelength is used to evaluate the

linear constant *n* and *k* for un-doped and Dy-doped Se-films using the Swanepoel method[14–16].

The dependence of the calculated linear optical constants *n* and *k*, on the applied wavelength for the studied samples is shown in **Figure 2**. In **Figure 2a** the Cauchy fitted values of *n* show a decrease against wavelength and an increase in the magnitude as the doping level of Dy increase in the structural network of a-Se. The dependence of the extinction coefficient (*k*) on λ shown in **Figure 2b** illustrates a decrease in exponential trend as λ increases and an increase against the doping content with Dy in a-Se films.

Figure 3 shows the refractive index as a function of composition for the investigated a-Se doped with Dy rare-earth ions films together with those published in literature at λ = 1.3 μm using different preparation techniques. The general trend of the function is the increase of *n* against Dy content ratio in at. %. However, the discrepancy among the data published by assorted authors is attributed to the variation in the preparation techniques used in formulating the studied materials in each reference besides the dependence of the properties of chalcogenides on its thermal history. In reference[17] bulk samples are prepared by conventional melt quenching technique for the mixture of the constituent elements. The obtained ingots are annealed at their glass transition temperature before any measurements. Furthermore, in reference[18] the obtained melt quenched ingots are used as source material to prepare thin film samples using KrF excimer laser operating at 248 nm.

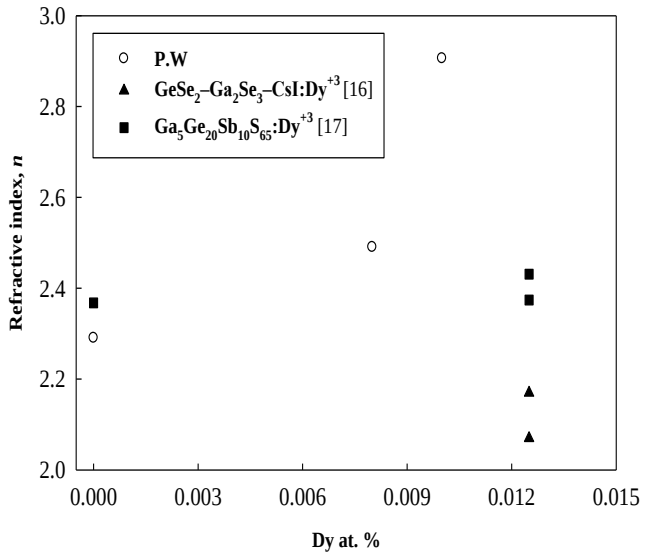

Figure 3. The variation of refractive index as a function of the doped Dy rare-earth ions in at. % for the present work [P. W.].

with those published in the literature[17,18].

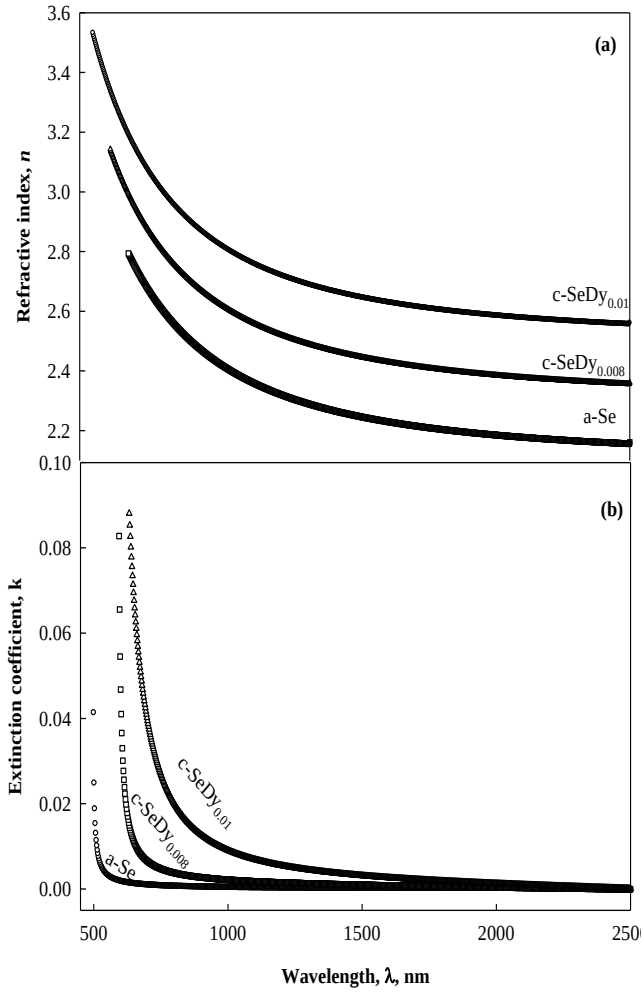

Figure 2. Variation of refractive index (*n*) (**a**) and extinction coefficient (*k*) (**b**) with wavelength (λ) for studied amorphous Se, c-SeDy$_{0.008}$ and c-SeDy$_{0.01}$ thin films.

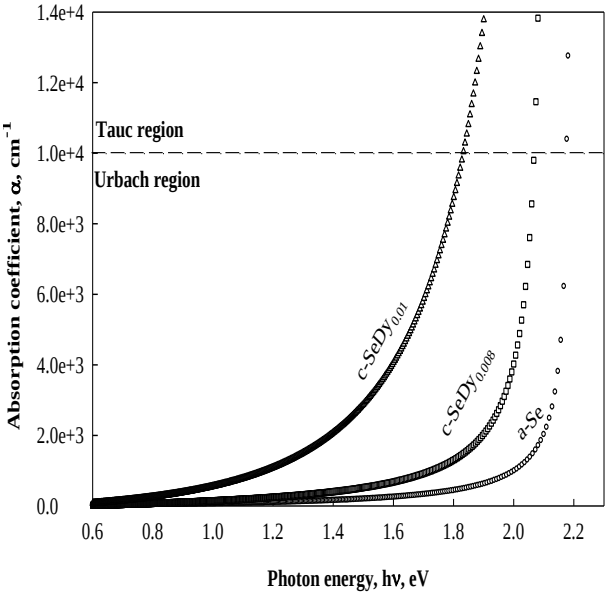

Figure 4. The calculated absorption coefficient (*α*) as a function of photon energy (*hν*) for the studied films. The dashed horizontal line differentiates between the Tauc and Urbach regions.

The dependence of the optical absorption coefficient (α) calculated using values of the extinction coefficient in **Figure 2b** on the incident photon energy of the investigated films is shown in **Figure 4**. This figure confirms that for all studied samples the value of α increases against photon energy in an exponential trend and shifted towards lower energy as doping rate increases in the structural network of a-Se films. This shift indicates that the absorption edge decreases in energy (redshift in wavelength) against the increase of doping level of Dy.

Each curve recognized in **Figure 4** could be divided into two different regions[19,20]:

The first region is for the high absorption, namely for $\alpha(h\nu) > 10^4$ cm^{-1} (Tauc region). The optical absorption in this region could be described by Tauc's relation[19]:

$$\alpha(h\nu) = A(h\nu - E_g)^r \quad (1)$$

where A is constant, E_g the optical band gap and r = 1/2 as well as 2 for direct and indirect transitions in sequence. According to Eq. (1), the dependence of $(\alpha h\nu)^{1/r}$ versus $h\nu$ is shown in **Figure 5** for both values of r. For each composition, the energy gap E_g is calculated by fitting the function $(\alpha h\nu)^{1/r} = f(h\nu)$, locally point by point to the linear regression line and extrapolating to $y = 0$ yields the value of E_g. The results are given in **Table 1** as a function of the film's composition. According to **Table 1**, it is observed that the value of optical band gap E_g decreases against an increase of Dy content through the considered range of doping 0.008-0.01 at. % of Dy.

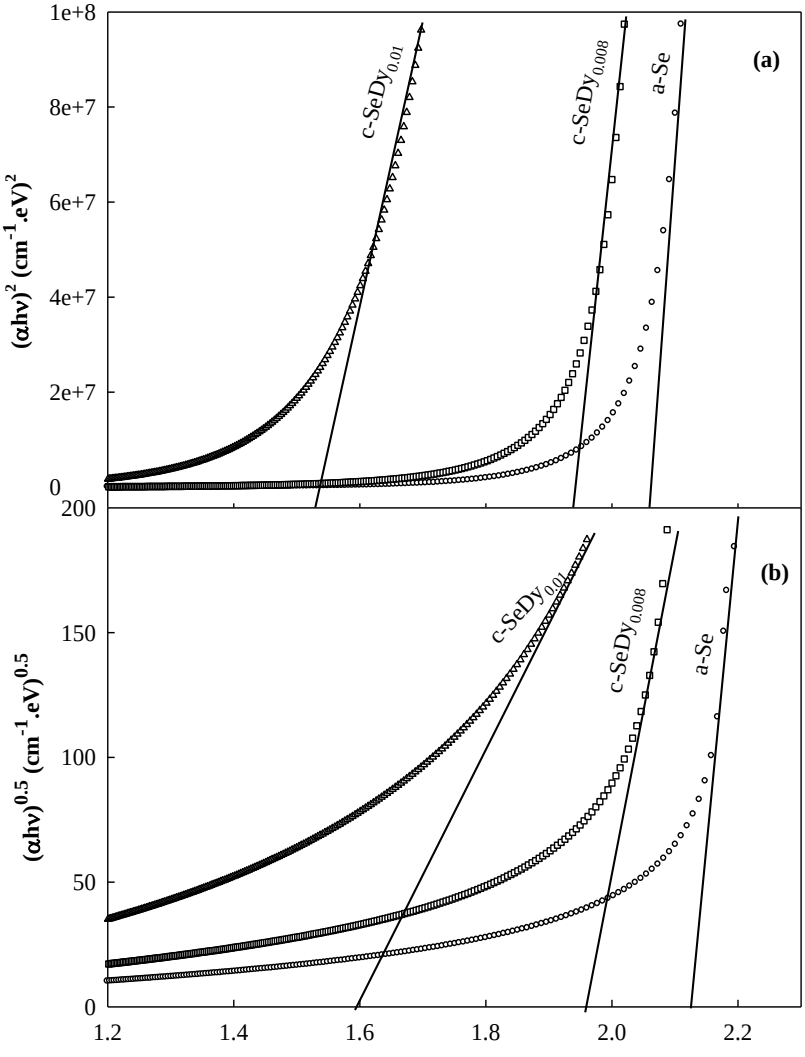

Figure 5. Tauc's plots for determining the optical energy gap of direct (**a**) and indirect (**b**) transitions for films investigated.

The decrease E_g against the increase of Dy content in the structure network of a-Se can be explained using the electronegativity of the elements involved. The electronegativity of Se and Dy are 2.55 and 1.22

respectively and Dy has a lower electronegativity than Se. The valance band of a-Se contains the lone pair p-electrons and the addition of an element with lower electronegativity (Dy) to a higher electronegative element (Se) may raise the energy of lone pair states, which is further responsible for the broadening of the valance band inside the forbidden gap and leads to band tailing and hence bandgap shrinkage[18].

The second region in **Figure 4** with $\alpha(h\nu) < 10^4$ cm^{-1} (Urbach region), where the absorption coefficient presents a roughly exponential behavior:

$$\alpha(h\nu) = \alpha_e \exp\left(\frac{h\nu}{E_u}\right) \quad (2)$$

Where α_e is a constant and E_u is an energy that is often interpreted as the width of the tail of localized states in the gap region. This relation was first proposed by Urbach[21]. The inverse slope or width of the exponential edge E_u reflects the width of the localized band tail[22] which is called Urbach energy. It determines the degree of disorder in the semiconductor which is responsible for internal potential fluctuations giving rise to tails of localized states at the band edges. The Urbach energy depends strongly on deposition conditions and annealing, which are likely to influence the disorder and therefore the band tailing[23]. The calculated values of E_u are given in **Table 1** as a function of film composition. These values show a decrease from 0.30 eV for the un-doped a-Se film to 0.25 and 0.21 eV for doping with 0.008 and 0.01 at. % in sequence. Such a decrease in the value of E_u indicates a decrease in the disordered character of a-Se due to the introduction of Dy which is consistent with the obtained structure using XRD for the studied samples shown in **Figure 1**. consequently, a decrease of E_u is attributed to the crystallized character of the thermally deposited films. Also, the existence of a band tail (E_u) that accompanied the localized states in the gap reflects some degree of disorder in the considered semiconductor film.

The complex dielectric constant $\varepsilon^* = \varepsilon_1 - i\varepsilon_2$ of a martial in terms of the linear optical constants, n, and, k, could be written as $\varepsilon_1 = n^2 - k^2$, $\varepsilon_2 = 2nk$ where ε_1 is the real part, while ε_2 is the imaginary part. **Figure 6** shows the calculated values of ε_1 and ε_2 of the complex dielectric constant versus the photon energy ($h\nu$)

Table 1. The calculated values of the optical energy gap, E_g, Urbach energy, E_u, high-frequency dielectric constant, ε_∞, the ratio of the free carriers density to the free carrier effective mass, N/m^* and plasma resonance frequency, ω_P, as a function of the studied film's composition

Film Composition	E_g, eV	E_u, eV	ε_∞	(N/m^*) x 10^{50} (cm^{-3} kg^{-1})	ω_p x 10^{14} Hz
a-Se	2.10	0.30	4.91	5.710	1.94
c-$SeDy_{0.008}$	1.96	0.25	5.54	6.079	2.48
c-$SeDy_{0.01}$	1.59	0.21	6.77	6.250	2.87

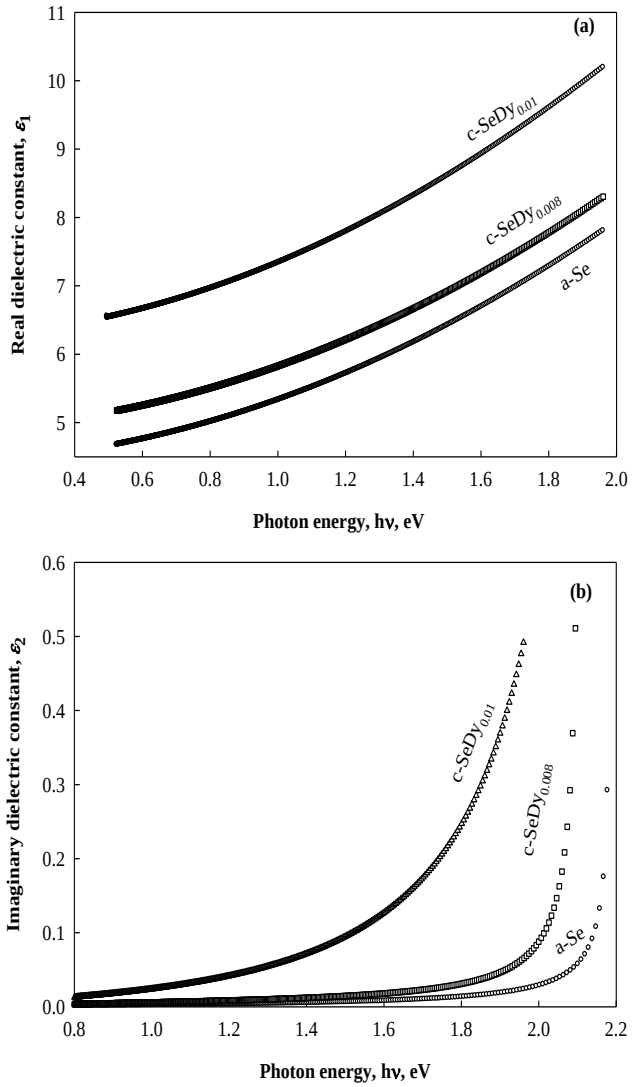

Figure 6. Real (**a**) and imaginary (**b**) parts of the dielectric constant versus photon energy for the films investigated.

for the present film's composition. **Figure 6a** shows a nearly exponential increase with photon energy for all investigated samples and nearly has the same trend as $n = f(\lambda)$. On the other hand, ε_2 illustrates a clear exponential increase of ε_2 against ($h\nu$) which has the same behavior as $k = f(h\nu)$. For a better

understanding of the optical behavior of the investigated films, it is necessary to determine some optical parameters such as dispersion of high-frequency dielectric constant and the lattice vibration modes as follows:

In the near-infrared spectral region, where the frequency is relatively low, the real ε_1 and imaginary ε_2 parts of the complex dielectric constant can be written as[24]:

$$\varepsilon_1 = \varepsilon_\infty - \frac{e^2}{4\pi^2 c^2 \varepsilon_0}\frac{N}{m^*}\lambda^2, \quad \varepsilon_2 = \frac{\varepsilon_\infty \omega_p^2}{8\pi^3 c^3 \tau}\lambda^3 \tag{3}$$

where ω_p is the plasma resonance frequency $\omega_p = \left(\frac{e^2 N}{\varepsilon_0 \varepsilon_\infty m^*}\right)^{\frac{1}{2}}$ of all the valence electrons involved in the optical transitions, ε_∞ the high-frequency dielectric constant, e electronic charge, c speed of light, ε_0 free space dielectric constant, N/m^* is the ratio of free carriers density to the free carrier effective mass and τ relaxation time. According to Eq. (3) plot of ε_1 versus λ^2 and extrapolating the linear part of the plot in the high wavelength region to zero wavelength gives the value of ε_∞ and the slope of this line is used to calculate values of (N/m^*) for the investigated films. The calculated ε_∞, (N/m^*) and ω_p are given in **Table 1** as a function of investigated film compositions. The value of N/m^* reflects an increase in the free carrier density with the increase of Dy-content which is argued to be the metal character of Dysprosium rare earth.

According to the single-effective oscillator model suggested by Wemple and DiDomenico[25], the refractive index could be described by the following relation:

$$n^2 - 1 = \frac{E_0 E_d}{E_0^2 - E^2} \tag{4}$$

where E is the photon energy in eV, E_0 is the single oscillator energy (average oscillator energy for electrons) and E_d is the dispersion energy parameter of the material. For the magnetic chalcogenides such as the present case of Dy doped Se films, Eq. (4) could be rewritten as[25]:

$$n^2 - 1 = \frac{\hat{E}_d \hat{E}_0}{\hat{E}_0^2 - E^2} + \frac{E_d E_0}{E_0^2 - E^2} \tag{5}$$

where $\hat{E}_d$, $\hat{E}_0$ applies to $f \rightarrow d$ transitions and E_d, E_0 applies to $s, p \rightarrow d$ transitions. It is straightforward to combine terms in Eq. (5) and get the following expressions for the equivalent single oscillator parameters $\bar{E}_0$ and $\bar{E}_d$[25]:

$$\bar{E}_0^2 = \hat{E}_0^2\left(\frac{1+\left(E_d/\hat{E}_d\right)\left(\hat{E}_0/E_0\right)}{1+\left(E_d/\hat{E}_d\right)\left(\hat{E}_0/E_0\right)^3}\right) \tag{6}$$

and

$$\bar{E}_d^2 = \hat{E}_d^2\left(\frac{\left[1+\left(E_d/\hat{E}_d\right)\left(\hat{E}_0/E_0\right)\right]^3}{1+\left(E_d/\hat{E}_d\right)\left(\hat{E}_0/E_0\right)^3}\right) \tag{7}$$

$\bar{E}_0$ is the dispersion energy parameter of the material and is a measure of the strength of interband optical transitions and $\bar{E}_d$ is related to the nearest neighbor cation coordination, anion valency, ionicity, and the effective number of dispersion electrons. According to Eq. (5) Plotting $(n^2\text{-}1)^{-1}$ versus the photon energy $(h\nu)^2$ as shown in **Figure 7** and fitting the straight part of the curve in the high energy region allows to obtain from the slope and the intercept values of E_0 and E_d. In the low energy region, the slope and intercept of the straight yields the values of $\hat{E}_d$ and $\hat{E}_0$. The calculated values of these dispersion parameters are listed in **Table 2**.

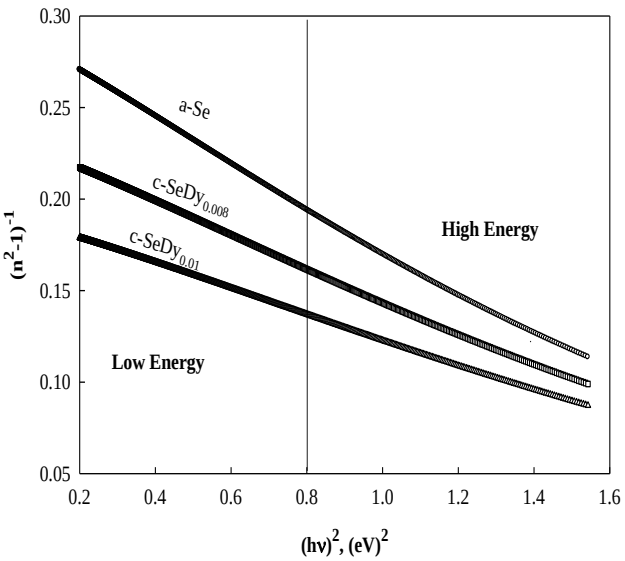

Figure 7. Plots of $(n^2\text{-}1)^{-1}$ versus $(h\nu)^2$ for the films investigated.

The estimated value of E_0 for a-Se (4.5 eV) is in good agreement with that reported by Wemple[26]. The results indicated that the average value of the single oscillator energy ($\bar{E}_0$) changed to 3.79 eV for c-$SeDy_{0.008}$ and 4 eV for c-$SeDy_{0.01}$. Such behavior of $\bar{E}_0$ could be attributed to the splitting of the sub-bands $5d(t_{2g}\text{-}e_g)$ by the crystal field and the

decrease of this splitting as well as the crystallized nature with increasing Dy-content.

If the wavelengths are much shorter than the phonon resonance, the lattice contribution is given by:

$$n^2 - 1 = \frac{\hat{E}_d \hat{E}_0}{\hat{E}_0^2 - E^2} + \frac{E_d E_0}{E_0^2 - E^2} - \frac{E_l^2}{E^2}, \quad (8)$$

where E_l is the lattice oscillator strength. Poignant[27] has shown that at a long wavelength, where $E^2 << \hat{E}_0^2$ and $E^2 << E_0^2$, a plot of $(n^2\text{-}1)$ versus $1/E^2$ approaches a straight line and Eq. (8) has the following form:

$$n^2 - 1 = \left(\frac{\hat{E}_d}{\hat{E}_0} + \frac{E_d}{E_0}\right) - \frac{E_l^2}{E^2} \quad (9)$$

The intercept of this line yield the ratio E_d/E_0 at high energy, and $\hat{E}_d/\hat{E}_0$ at low energy, while the slope is $-E_l^2$. The obtained values of E_l are given in **Table 2**. The tabulated values of E_l shows variation from 0.54 eV for a-Se to 0.36 eV for c-$SeDy_{0.008}$, and 0.38 eV for c-$SeDy_{0.01}$ respectively.

Table 2. Values of single oscillator energy (E_0, $\bar{E}_0$), dispersion energy (E_d, $\bar{E}_d$) lattice oscillator strength (E_l), and wavelength at zero material dispersion (λ_c) for investigated films composition

Film Composition	E_0, eV	E_d, eV	$\hat{E}_0$, eV	$\hat{E}_d$, eV	$\bar{E}_0$, eV	$\bar{E}_d$, eV	E_l, eV	λ_c, µm
a-Se	4.50	24.25	-----	-----	------	-----	0.54	1.60
c-$SeDy_{0.008}$	3.74	12.62	2.49	6.34	3.97	8.36	0.36	1.66
c-$SeDy_{0.01}$	3.18	11.66	2.17	5.45	4.00	12.65	0.38	1.74

The material dispersion $M(\lambda)$ could be expressed in terms of the refractive index, n, as:

$$M(\lambda) = \frac{\lambda}{c}\left(\frac{d^2 n}{d\lambda^2}\right) \quad (10)$$

Differentiating Eq. (8) w.r.t λ yields the material's dispersion as a function of $\bar{E}_0$ and $\bar{E}_d$ as follows[26]:

$$M(\lambda) = 1.54\times10^4 \frac{\bar{E}_d / \bar{E}_0^3}{n\lambda^3} - 2.17\times10^3 E_l^2 \frac{\lambda}{n} \quad (ps\,nm^{-1}km^{-1}) \quad (11)$$

Figure 8 shows the graphical relation of the calculated $M(\lambda)$ versus wavelength. The wavelength at which $M = 0$, and the obtained results are given in **Table 2** as a function of films composition. Similarly, the value of λ_c can be calculated from Wemple's three-parameter formula[26]:

$$\lambda_c = 1.63\left(\frac{\bar{E}_d}{\bar{E}_0^3 \bar{E}_l^2}\right)^{\frac{1}{4}} \quad (12)$$

Nevertheless, the observed variation of λ_c indicates that the introduction of Dy atoms in a-Se causes a shift of the material dispersion $M(\lambda)$ towards higher wavelengths. Such a redshift represents an important parameter to improve the operational conditions and performance of optical fibers[28,29]. Indeed, the listed values of material dispersion in **Table 2** show that

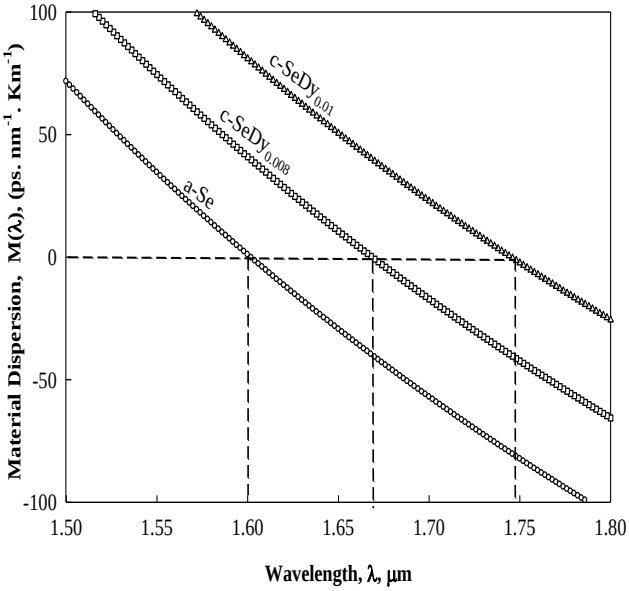

Figure 8. Variation of the material dispersion versus wavelength for the films investigated.

the pumping of optical signals in the Selenium chalcogenide fibers at zero dispersion wavelength (ZMD) could be tuned by increasing the doping ratio of Dy[30,31].

3.2 Non-Linear optical dispersion

The microscopic nonlinear properties of the chalcogenide semiconductors have been investigated through the determination of second-order refraction index, n_2 and nonlinear absorption coefficient β,

where n_2 and β are expressed as

$$n_t = n + n_2 I \quad (13)$$

and

$$\alpha(I) = \alpha + \beta I,$$

where I is the incident intensity, n_t is the total refractive index and n represents the weak-field refractive index (linear refractive index). The second-order index of refraction, n_2 is required for soliton propagation in the optical telecommunication fibers and used in all-optical switching schemes.

Boling *et al.*[32] derived a semi-empirical relation for predicting the second-order index of refraction, n_2, for semiconductors from the linear refractive index, n which has the simplest form:

$$n_2(\times 10^{-13} esu) = G\frac{n-1}{\nu_d^{5/4}} \quad (14)$$

where G is an empirical constant and G = 391[32]. Here ν_d is the Abbe dispersion number and is given by:

$$\nu_d = \frac{n_d - 1}{n_F - n_C} \quad (15)$$

where n_d, n_F, and n_C refer to refractive indices at 589.0, 486.1, and 656.3 nm respectively.

The two-photon absorption coefficient β is given by[33]:

$$\beta = \frac{KE_p^{1/2}F(2h\nu/E_g)}{n^2E_g^3} \quad (16)$$

where K is the material-independent constant given by

$$K = \frac{2^9\pi}{5}\frac{e^4}{c^2\sqrt{m_o^*}} \quad (17)$$

Here e and m_o^* are the electron charge and its effective mass, respectively. In our calculations, K = 3100 and E_p is related to the Kane momentum parameter, p, where $E_p = 2p^2m/h^2$ and m is the electron mass. F is a function that represents the dispersion of β with respect to the incident photon energy $h\nu$. This function depends upon the band structure and determines the energy states that are coupled. The function F can be evaluated from the relation[33]:

$$F(2h\nu/E_g) = \frac{[(2h\nu/E_g)-1]^{3/2}}{(2h\nu/E_g)^5} \quad (18)$$

The overall dispersion behavior of β, as shown in **Figure 9b** a ratio between the maximum nonlinear absorption coefficients of the two-photon absorption (TPA) to the optical bandgap energy equals 1.4 is observed for different chalcogenide compositions[34–40]. The maximum nonlinear absorption coefficient β for investigated films is given in **Table 3**. The dispersion of $n_2 = f(h\nu)$ is be plotted as shown in **Figure 9a**.

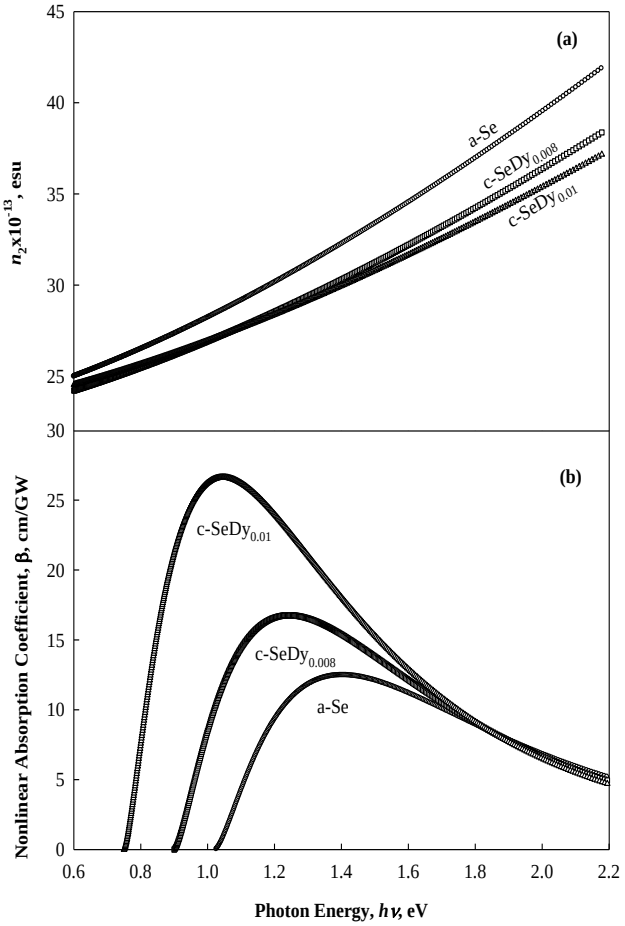

Figure 9. Dependence of second-order refractive index, n_2 (**a**) and nonlinear absorption coefficient, β (**b**) on the incident photon energy, $h\nu$ for the studied films.

Table 3. The nonlinear absorption coefficient, β_{max}, values of the energy corresponding to β_{max}, $E_{\beta = max}$, the ratio of $E_g/E_{\beta = max}$ for the studied samples

Film Composition	β_{max} cm/GW	$E_{\beta = max}$ eV	$E_g/E_{\beta = max}$
a-Se	13.6006	1.4739	1.42
c-SeDy$_{0.008}$	16.7625	1.3805	1.42
c-SeDy$_{0.01}$	26.631	1.1197	1.42

4. Conclusion

The study of the role played by dysprosium ions as a dopant in the structural network of a-Se on optical dispersion leads to draw the main following concluding remarks:

The optical band gap (E_g) decreases with an increase of the Dy content which is argued to be the difference in electronegativity between Se and Dy.

The variance between the values of the optical energy gaps of the studied samples and previously published data for other chalcogenide compositions doped also with Dy are attributed to the sensitivity of chalcogenides to its thermal history and preparation conditions.

The single oscillator energy, E_o, showed a decrease accompanied by an increase in the values of E_d. This trend of E_o and E_d shifted the material dispersion $M(\lambda)$ towards longer wavelengths from 1.6 to 1.74 nm against the increase in the Dy-content. This shift means that the material dispersion of chalcogenide fiber could be tuned by controlling the doping ratio of Dy.

A ratio between the maximum nonlinear absorption coefficients of TPA to the optical bandgap energy equals 1.4 is observed for different chalcogenide semiconductors.

Conflict of interest

The authors declare that they have no conflict of interest.

References

1. Yang Z, Chen W, Luo L. Dy^{3+}-doped Ge-Ga-Sb-Se glasses for 1.3 μm optical fiber amplifiers. Journal of Non-Crystalline Solids 2005; 351(30-32): 2513–2518.
2. Heo J. 1.3 μm-emission properties and local structure of Dy^{3+} in chalcohalide glasses. Comptes. Rendus Chimie 2002; 5(11): 739–749.
3. Hewak DW, Samson BN, Medeiros Neto JA, *et al*. Emission at 1.3 μm from dysprosium-doped Ga:La:S glass. Electronics Letters 1994; 30(12): 968–970.
4. Wei K, Machewirth DP, Wenzel J, *et al*. Spectroscopy of Dy^{3+} in Ge-Ga-S glass and its suitability for 1.3 μm fiber-optical amplifier applications. Optics. Letters 1994; 19(12): 904–906.
5. Tang G, Yang Z, Luo L, *et al*. Dy^{3+}-doped chalcohalide glass for 1.3-μm optical fiber amplifiers. Journal of Materials Research 2008; 23(4): 954–961.
6. Mott NF, Davis EA. Electronic Processes in Non-Crystalline Materials, 2nd ed. Oxford, New York: Oxford University Press; 1979.
7. Elliott SR. Physics of Amorphous Materials. 2nd ed. New York: Longmann Scientific & Technical; 1990.
8. Zakery A, Elliott SR. Optical Nonlinearities in chalcogenide glasses and their applications. NY: Springer Berlin Heidelberg; 2007.
9. Park BJ, Seo HS, Ahn JT, *et al*. Dy^{3+} doped Ge-Ga-Sb-Se glasses and optical fiber for the mid-IR gain media. Journal of the Ceramic Society of Japan 2008; 116(1358): 1087–1091.
10. Heo J. Rare-earth doped chalcogenide glasses for fiber-optic amplifiers. Journal of Non-Crystalline Solids 2003; 326 & 327: 410–415.
11. Shen Z, Li Y, Hu Q, *et al*. Dielectric properties of B–site charge balanced Dy–doped SrTiO ceramics for energy storage. Journal of Electroceramics 2015; 34: 236–240.
12. Abdel-Wahab FA, Maksoud HA. Electrical conduction and dielectric relaxation in selenium films doped with dysprosium rare earth. American Journal of Condensed Matter Physics 2017; 7(2): 41–49.
13. Pamuckchieva V, Szekeres A. Optical properties of $Ge_xSb_{20-x}Te_{80}$ thin films and their changes by light illumination. Optical Mater. 2008; 30(7): 1088–1092.
14. Boycheva S, Sytchkova AK, Bulir J, *et al*. Optical constants of As_2Se_3–Ag_4SSe–SnTe amorphous thin films. Journal of Non- Crystalline Solids 2007; 353: 1618–1623.
15. Swanepoel R. Determination of the thickness and optical constants of amorphous silicon. Journal of Physics. E: Scientific Instruments 1983; 16(12): 1214.
16. Swanepoel R. Determination of surface roughness and optical constants of inhomogeneous amorphous silicon films. Journal of Physics E: Scientific Instruments 1984; 17(10): 896.
17. Tang G, Yang ZY. Dy^{3+}-doped chalcohalide glass for 1.3-μm optical fiber amplifiers. Journal of Materials Research. 2008; 23(4): 954–961.
18. Nazabal V, Němec P, Jedelský J, *et al*. Dysprosium doped amorphous chalcogenide films prepared by pulsed laser deposition. Optical Materials 2006; 29(2-3): 273–278.
19. Tauc J, Grigorovici R, Vacu A. Optical Properties and Electronic Structure of Amorphous Germanium. Physica Status Solidi 1996; 15(2): 627–637.
20. Tauc J. Amorphous and Liquid Semiconductors. Plenum, New York; 1974.
21. Urbach F. The Long-Wavelength Edge of Photographic Sensitivity and of the Electronic Absorption of Solids. Physical Review 1953; 92: 1324–1325.
22. Redfield D. Energy-band tails and the optical absorption edge; the case of a-Si:H. Solid State Communications 1982; 44(9): 1347–1349.
23. Theye ML. Non-Crystalline semiconductor. Vol. 2, M. Pollak. CRC Press: 1987.
24. Moss TS, Burrell GJ, Ellis E. Semiconductor Opt-Electronics. London: Butterworths-Heinemann; 1973.
25. Wemple SH, DiDomenico M. Behavior of the electronic dielectric constant in covalent and ionic materials. Physical Review B 1971; 3(4): 1338–1351.
26. Wemple SH. Material dispersion in optical fibers.

Applied Optics 1979; 18(1): 31–35.
27. Poignant H. Dispersive and scattering properties of a ZrF4 based glass. Electronics Letters 1981; 17(25-26): 973–974.
28. Nassau K, Wemple SH. Material dispersion slope in optical fiber waveguides Electron. Electronics Letters 1982; 18(11): 450–451.
29. Boyd RW. Nonlinear Optics. 4th ed. Academic Press; 1992.
30. Klimczak M, Siwicki B, Skibinski P, *et al*. Coherent supercontinuum generation up to 2.3 μm in all-solid soft-glass photonic crystal fibers with flat all-normal dispersion. Optics Express 2014; 22(15): 18824–18832.
31. Lui L, Cheng T, Nagasaka K, *et al*. Coherent mid-infrared supercontinuum generation in all-solid chalcogenide microstructured fibers with all-normal dispersion. Optics Letters 2016; 41(2): 392–395.
32. Boling NL, Glass AJ, Owyoung A. Empirical relationships for predicting nonlinear refractive index changes in optical solids. IEEE Journal of Quantum. Electronics 1978; 14(8): 601–608.
33. Abdel-Wahab FA, El-Diasty F, Abdel-Baki M. Dispersion dependence of second-order refractive index and complex third-order optical susceptibility in oxide glasses. Physics Letters A 2009; 373(42): 3855–3860.
34. Quémarda C, Smektala F, Couderc V, *et al*. Chalcogenide glasses with high nonlinear optical properties for telecommunications. Journal of Physics and Chemistry of Solids 2001; 62(8): 1435–1440.
35. Smektala F, Quemard C, Leneindre L, *et al*. Chalcogenide glasses with large non-linear refractive indices. Journal of Non-Crystalline Solids 1998; 239(1-3): 139–142.
36. Rangel-Rojo R. Kimura K, Matsuda H, *et al*. Dispersion of the third-order nonlinearity of a metallo-organic compound. Optics Communications 2003; 228(1-3): 181–186.
37. Petit L, Carlie N, Villeneuve R, *et al*. Effect of the substitution of S for Se on the structure and non-linear optical properties of the glasses in the system $Ge_{0.18}Ga_{0.05}Sb_{0.07}S_{0.70-x}Se_x$. Journal of Non-Crystalline Solids 2006; 352(50-51): 5413–5420.
38. Zakery A, Elliott SR. Optical properties and applications of chalcogenide glasses: A review. Journal of Non-Crystalline Solids 2003; 330(1-3): 1–12.
39. Petkov K, Ewen PJS. Photoinduced changes in the linear and non-linear optical properties of chalcogenide glasses. Journal of Non-Crystalline Solids 1999; 249(2-3): 150–159.
40. Requejo-Isidro J, Mairaj AK, Pruneri V, *et al*. Selfrefractive non-linearities in chalcogenide based glasses. Journal of Non-Crystalline Solids 2003; 317(3): 241–246.